9950-540

DOE/JPL
Distribution Category UC-6
Report #6

DEFECT STRUCTURE OF EFG SILICON RIBBON

December 1980

JPL Contract No. 954852

by

H. Strunk[†], B. Cunningham and D. Ast

Materials Science and Engineering
Bard Hall, Cornell University
Ithaca, New York 14853

The JPL low-cost solar array project is sponsored by the U.S. Department of Energy and forms part of the Solar Photovoltaic Conversion Program to initiate a major effort toward the development of low-cost solar arrays. This work was performed for the Jet Propulsion Laboratory, California Institute of Technology by agreement between NASA and DOE.

[†] Permanent address: Max Planck Institut für Metallforschung, Institut für Physik, 7000 Stuttgart 80, FRG.

DEFECT STRUCTURE OF EFG SILICON RIBBON

by

H.Strunk†, B. Cunningham and D. Ast
Materials Science and Engineering
Bard Hall, Cornell University
Ithaca, New York 14853

ABSTRACT

The defect structure of EFG ribbons has been studied using EBIC, TEM and HVEM. By imaging the same areas in EBIC and HVEM a direct correlation between the crystallographic nature of defects and their electrical properties has been obtained. (i) Partial dislocations at coherent twin boundaries may or may not be electrically active. Since no microprecipitates were observed at these dislocations it is likely that the different electrical activity is a consequence of the different dislocation core structures. (ii) 2nd order twin joins were observed which followed the same direction as the coherent first order twins normally associated with EFG ribbons. These 2nd order twin joins are in all cases strongly electrically active.

EFG ribbons contain high concentrations of carbon. Since no evidence of precipitation was found with TEM it is suggested that the carbon may be incorporated into the higher order twin boundaries now known to exist in EFG ribbons.

† Permanent address: Max Planck Institut für Metallforschung, Institut für Physik, 7000 Stuttgart 80, FRG.

1. INTRODUCTION

Rapid progress has recently been made in the production process of edge defined film-fed growth (EFG) silicon /1/. EFG ribbon is a promising material for the production of inexpensive solar cells and therefore an understanding of the relationship between the crystallographic nature of the defects and their electrical properties is desirable. This information can then hopefully be used to modify the ribbon growth process to reduce the density of defects which decrease the efficiencies of solar cells.

After a summary of the characteristic defect structure of various EFG silicon ribbons, results are presented which were obtained by correlating EBIC measurements and HVEM observations on selected defects.

2. EXPERIMENTAL TECHNIQUES

The electrical properties (i.e. enhanced minority carrier recombination) were investigated in the scanning electron microscope (SEM) operated in the electron beam-induced current (EBIC) mode. Schottky diodes were produced by evaporating a thin film of Al($\sim$500Å) onto one surface /2/. EBIC images exhibit dark contrast at defects which act as recombination sites for minority carriers, with an EBIC resolution of $\sim$1-2µm. The EBIC technique can be extended to obtain quantitative information. The collected current can be measured as a function of specimen co-ordinates allowing the determination of 'recombination efficiencies' of specific defects /3/, minority carrier lifetime /4/ and trap level measurements /5/ are possible using high speed beam blanking techniques. These extensions of the EBIC technique are currently being introduced.

Defect structures were investigated by transmission electron microscopy (TEM). To obtain unbiased observations, specimens were broken off the ribbons at random, ground to a thickness of $\sim$50µm and thinned for TEM examination by ion beam milling. Subsequent investigations were carried out in a Siemens Elmiskop 102 operating at an accelerating voltage of 125 kv (conventional TEM, CTEM).

To correlate electrical and structural properties of defects, areas were selected and mapped out in EBIC. Specimens 3mm in diameter were then cut out from the ribbon and ion-milled from the back-side (with the Schottky-diodes still at the surface) until the areas of interest were contained in the electron transparent regions. These specimens were subsequently examined in a high-voltage electron microscope (HVEM) operating at an accelerating voltage of 1MV. HVEM has the following advantages over CTEM because of the high penetration power of highly accelerated electrons (several μm as compared to 0.5μm in CTEM):

(i) The probability of finding the defects, previously mapped by EBIC, in the large transmittable area is high.

(ii) Extended defects such as twin or other grain boundaries can easily be traced over long distances.

(iii) The volumes investigated by HVEM and by EBIC are comparable.

Difficulties arise when comparing EBIC and HVEM micrographs because of the large difference in working magnifications (SEM-EBIC typically 1,000x, HVEM typically 10,000x). The comparison is facilitated by utilizing permanent surface marks, such as scratches, or etched topological features. In addition a series of low magnification EBIC micrographs (10x, 50x, 200x) helps to locate the areas of interest.

A brief discussion of the advantages of the present technique for the electrical characterization of defects, may be found in /6/.

3. INVESTIGATED EFG RIBBONS

The ribbons investigated in the present study are briefly described below:

1) JPL identification #5-871 run 18-112-1, 'small grain'. Displaced die, growth speed 3.0-3.4 cm/min. Undoped.

2) JPL identification #5-866 run 16-163, 'small grain'. Displaced bulbous ended die, growth speed 3.1 cm/min. Boron doped, resistivity 1Ωcm.

3) JPL identification #5-1158. 'Large grain'. (reduced ΔT flow).

4) Mobil Tyco supplied...'large grain' ribbon. (reduced ΔT flow).

4. CHARACTERISTIC DEFECT STRUCTURE OF EFG SILICON RIBBONS

4.1. Etch

Similar features were observed in all of the EFG ribbons examined, the only difference being the scale of the defects (e.g. 'large' and 'small' grain). Figs. 1(a) and (b) show typical etch patterns, which have already been described (e.g. /7/to/10/). Only a brief description will therefore be given here, with emphasis on features which are interesting in connection with the correlation work reported in Section 5.

On a large scale the observed pattern is generally inhomogeneous, on a small scale, however, frequently homogeneous. Figure 1(a) shows an area of parallel striations, which are generally attributed to the presence of twin boundaries. (see Section 5 for a detailed discussion). At the top of Figure 1(a) is a region containing a high density of dislocation etch pits. It should be noted that the density of dislocations varies appreciably from region to region. Whereas Figure 1(a) represents the 'standard' defect structure (i.e. equilibrium structure', e.g. /11/) which is frequently discussed, Figure 1(b) shows an example of a more complicated pattern. Areas such as this were found on all of the ribbons and covered appreciable areas of the surface. The irregularity in Figure 1(b) is caused by reactions between grain and/or twin boundaries and by an inhomogeneous distribution of dislocations. In several regions the dislocation etch pits are aligned along crystallographic directions suggesting that the dislocations had been generated by plastic processes (See Section 5).

The orientation of the grains at the surface varies; in order of falling frequency {110}, {112} have been found, in partial agreement with earlier work /12,13/. An example of the variation in grain orientation is shown in Figure 2. Orientations are given with respect to the growth direction.

4.2. EBIC

Figure 3 is a low magnification EBIC micrograph showing the distribution of electrically active defects. In the upper part of the micrograph contrast lines apparently due to grain boundaries are visible. In addition black dots due to active dislocations are randomly distributed throughout the matrix. [Figure 4 is a higher magnification micrograph of the area described above.] Most of Figure 3 consists of almost horizontally aligned boundaries, some of these very dark (showing strong electrical activity), some weak in contrast or exhibiting 'dotted' contrast. Figure 5 shows an-

other example of dotted EBIC contrast where the effect is more pronounced. We will show in Section 5 that this pattern is related to the twinned structure of the material. Such a relationship was earlier inferred from comparison of etched surfaces and EBIC micrographs /3/ and by independent observations of twins in TEM /10/. An exact analysis, however, requires direct correlation between EBIC and TEM, as presented in Section 5.

4.3. TEM

Twins with a {111} habit plane occur with a high frequency and are therefore generally observed by TEM. A typical twinned structure is shown in Figure 6. The thicknesses of micro-twins may vary from a few layers of {111} planes up to tens of microns (which of course means single twin boundaries are observed in TEM). A microtwin five layers thick is revealed by structural imaging in Figure 7. The 'small grain' ribbons contain a high density of microtwins (e.g. Figure 6) with thicknesses up to several 100 nm. 'Large grain' material contains isolated twin boundaries spaced several µm apart, resulting in a more proportionate distribution of 'twinned' and 'matrix' material.

Twin boundaries may contain partial dislocations (twin boundary dislocations) the density of which can vary from boundary to boundary. No relationship between twin boundary dislocation density and ribbon type has been found.

4.4. Results concerning the carbon content

Graphite dies are used in EFG ribbon growth. Two consequences result from this technique: (i) SiC - particles are present at the ribbon surface (e.g. /3/) and (ii) a high density of carbon ($\sim 10^{18} - 10^{19} cm^{-3}$ /14/) is incorporated into the silicon material.

EBIC has been used to investigate the electrical activity of the defect structure nucleated at SiC particles. Figure 8 shows a typical arrangement with a high density of black dots, corresponding to dislocations, and a number of twin boundaries. Except for this high density of defects no other unusual effects were observed. This is particularly interesting since an excess of carbon may be expected near a SiC particle, thereby enhancing any carbon-induced impurity segregation. Such a segre-

gation is expected to cause increased minority carrier recombination. However, in the present study, the electrical activities of the defect structure near SiC particles, and of the 'equilibrium structure' are not noticeably different.

Recently a ribbon growth model was proposed to account for carbon concentrations above the solubility limit /15/. The model assumes eutectic growth and directional solidification of the ribbon, which leads to lamellae of a silicon-carbon 'phase' embedded in a carbon rich silicon matrix. Such a structure should give rise to special contrast effects in TEM. If the silicon-carbon phase is not coherent with the silicon matrix, which is likely due to the difference in the bond lengthsof silicon and carbon atoms, strain contrast effects should be observed, at least at irregularities of the lamellae. Moreover, interference patterns, e.g. Moiré fringes, and/or, in the case of a long range order, diffraction effects would be expected. None of these effects has been observed in this study.

5. CORRELATION OF EBIC WITH HVEM OBSERVATIONS

Figure 9(c) shows part of an EBIC micrograph exhibiting a row of dots similar to those seen in Figure 3. Figure 9 (a) is a HVEM micrograph of the same area. A comparison of Figure 9 (a) and (c) confirms that the dots mark the trace of a microtwin approximately 200 nm thick, the boundaries of which are visible in fringe contrast. This microtwin is imaged in Figure 9 (b) with its boundaries invisible, revealing that partial dislocations are contained in both boundaries. A comparison of EBIC and HVEM micrographs shows a one to one correspondence between dots and dislocations. Ignoring the central spot for the moment, the EBIC dots have similar contrast and correspond to individual, slightly curved dislocations. Diffraction contrast analysis reveals that the dislocations differ in Burgers vector (of type 1/6 <112>), and that their character is not of simple 30° or 90° type. These observations suggest that the dislocations are comparably effective sites for the recombination of minority carriers, irrespective of their crystallographic character. The central dot in Figure 9 (c) arises from the combined effect of a group of 3 partial dislocations which are too closely spaced to be resolved by EBIC. ($\sim$1-2μm).

Figure 10 (a) shows another example of dots in EBIC contrast. These dots, though similar to those shown in Figure 9 (c) are caused by a totally different structure. Figure 10 (b) is an etch pattern from the same area, showing that the observed contrast in Figure 10 (a) is due to the interaction of boundaries. The nature of the boundaries was determined by HVEM. As an example the area encircled in Figure 10 is shown in Figure 11. A three dimensional sketch of this area clarifying the relationships between the different areas is given in Figure 12. Analysis shows that T_1 is a microtwin ∿100nm thick, lying in the matrix M perpendicular to the growth surface. T_2 is in a different twin orientation to the matrix M with an inclined {111} - habit plane. Thus the boundary between T_1 and T_2 joins two crystal grains with a misorientation caused by two non-parallel twinning operations. The geometric construction is depicted in Figure 13, projected along the <110> direction common to all three grains. Boundaries of this type have been termed 'second order twin joins' by Kohn /16/ and are Σ9 boundaries in the CSL model /17/. In the present case the {111} plane of T_1 matches a {115} plane of T_2. This unsymmetric configuration has been modelled by Kohn /18/, yet has not been observed so far to the author's knowledge. The dislocation model discussed by Hornstra /19/ could also be extended to describe this unsymmetric case, but would require a very high density such that the dislocation core regions would overlap. In Figure 11 (b) the specimen was tilted to show the boundaries of the microtwin T_1. Dislocations that are contained in the {111}/{115} boundary are clearly visible. These dislocations accommodate a small deviation from the {111}/{115} orientation relationship and are commonly referred to as extrinsic boundary dislocations /20/. The Burgers vectors of these dislocations have not been analyzed.

Figure 14 shows a contrast experiment to determine the character of the partial dislocations present in the boundaries T_2/M. The specimen was tilted until these boundaries were almost perpendicular to the incident electron beam, allowing an easy determination of the crystallographic direction of the straight dislocation lines. The Burgers vectors were found from standard contrast analysis /21/. The dislocations

analyzed were Shockley partials of either 30° or 90° type, examples are indicated in Figure 14 (c).

The comparison of the HVEM micrographs (Figures 11 and 14) with the corresponding EBIC pattern (Figure 10) gives the following result: (i) The black dots in Figure 10 (a) correspond to the {111}/{115} second order twin joins, which therefore represent efficient sites for minority carrier recombination. (ii) The straight 30° and 90° partial dislocations show no contrast in EBIC (although etched in Figure 10 (b)) and thus are virtually electrically inactive.

6. DISCUSSION

In recent years a large number of experimental results on the dislocation core structure in tetrahedrally co-ordinated semiconductors has appeared (e.g. /22/). High resolution electron microscopy has revealed the presence of dissociated and constricted perfect dislocations (e.g. /23, 24/). Dislocations introduced by plastic processes are generally dissociated /22/ and are, since dissociation is difficult to envisage on the shuffle-set, therefore assigned to the glide set (e.g. /22/). Indications for the existence of "shuffle set" dislocations /25/ in Ge, suggest that such dislocations also may exist in Si. Transformation from one set to the other can occur by the addition or removal of rows of point defects /26/; experimental evidence for such a process exists (e.g. /24/).

Theoretical models for dislocation core structures were first developed by Hornstra /27/, and these models have been extended and refined to include bond reconstruction (e.g. /23/). The electrical properties of dislocations with different core structures are likely to be different.

Experimental results obtained by combining EBIC with HVTEM will contribute to the discussion of these various models.

6.1. Dislocations at coherent twin boundaries

In the present investigations dislocations were observed with apparently two different levels of electrical activity: dislocations giving rise to an EBIC contrast, Figure 9 (c), and dislocations with no, or at least considerably lower electrical activity, Figure 11. Confirmation of these observations is required before a detailed inter-

pretation of the nature of dislocations can be presented. It is however interesting to speculate about the possible significance of the present results, with regard to the formation and core structures of dislocations.

The simplest approach to correlating crystallographic and electrical properties is to reduce the number of applicable models. To this end the present investigation is concerned with single partial dislocations and therefore the question of whether the dislocation is dissociated or constricted (as present with perfect dislocations) does not arise.

It is conceivable that the core structure of a dislocation will depend on how the dislocation is generated. The present observations, that the electrically active dislocations do not follow <110> directions, and are in fact sometimes curved, and that the non-active dislocations are aligned along a <110> Peierls valley, tends to support this view. During growth of EFG ribbons there are two temperature ranges in which dislocation generation processes may occur. During solidification, when diffusion can occur, twin boundaries grow and can accomodate partial dislocations by atomic steps in the boundaries. At lower temperatures thermal stresses are relieved by plastic processes and these dislocations can react with twin boundaries, in which case the lattice dislocations dissociate into twin-boundary partial dislocations. Diffusion plays only a minor role in this case. Whether a distinction between grown-in and deformation induced dislocations is possible and what type of dislocations are formed by each process has yet to be determined.

6.2. The {111} {115} second order twin join

The present study has shown that the detected {111} {115} second order twin join is strongly electrically active. Since extrinsic dislocations are contained in the investigated boundary it cannot be explicitly stated that the electrical activity is an intrinsic property of the boundary. However considering the complicated arrangement of atoms and bonds at the boundary (e.g. Figure 13) it is likely that the extrinsic dislocations have only an additional effect, if at all, on the electrical activity.

Since the second order twin join is confined to the {111} matrix planes it is of

considerable interest in the discussion of the so-called equilibrium structure /11/ of EFG (and comparably grown) ribbons. This structure has been identified from etch investigations to be generally present in EFG ribbons and to consist of parallel coherent twin boundaries which extend on {111} matrix planes along the growth direction. Consequently, once a second order twin join is formed on a {111} matrix plane it can extend over long distances parallel to the equilibrium structure without further reactions. Second order twin join therefore have to be regarded as an inherent part of the defect structure of EFG ribbons. Thus the equilibrium structure consists of a large number of electrically inactive coherent twin boundaries intermingled with electrically active second (or even higher) order twin joins. This conclusion is consistent with thus far unexplained EBIC observations (e.g. /3, 10/, that only some of the linear boundaries revealed by etching are electrically active.

6.3. CARBON DISTRIBUTION IN EFG-RIBBONS

It has been found that the grain size of EFG ribbons generally decreases with increasing (overall) carbon concentration /15/. Since this concentration is beyond the carbon solubility limit in silicon the distribution of C has to be considered. The present experiments give no indication for a lamellae two-phase structure as suggested in the eutectic growth model /15/. The TEM observation of {115} {111} second order twin joins suggests the possibility that the carbon is preferentially incorporated into such joins, as well as into higher order twin and other grain boundaries. This explanation seems reasonable since the atomic arrangement at these boundaries is considerably disturbed (independent of the model used to describe the joins) thereby allowing the incorporation of a high density of carbon atoms. The correlation-higher carbon concentration smaller grain size is natural in this context since decreasing grain size increases the possibility of twin boundary interactions. How an intentional increase in the concentration of incorporated carbon atoms (by changing the growth conditions of the EFG ribbon) causes more boundaries to form, and how the carbon atoms influence the electrical activity of the higher order twin joins are topics of future research.

CONCLUSIONS

1. The correlation of HVTEM and EBIC is a valuable tool for the investigation of the defect structure of semiconducting materials, e.g. EFG ribbons.
2. The existence of the {115} {111} second order twin join has been proven for the first time. It may occur relatively frequently in the ribbon due to twin boundary interactions and lies along the same direction as the first order twin boundaries.
3. The {115} {111} twin joins were observed to be electrically active, whereas coherent {111} {111} twin boundaries were inactive.
4. Partial dislocations at coherent twin boundary can be electrically active. No microprecipitates were observed at these dislocations suggesting that the electrical activity is not impurity controlled but a consequence of the dislocation core structure per se.
5. It is suggested that the carbon atoms present in EFG ribbons in high concentrations are preferentially adsorbed to the higher order twin joins.

REFERENCES

1. J.P. Kalejs, B.H. Mackintosh and T. Surek, J. Cryst. Growth, 50 175 (1980).
2. T. Sullivan and D.G. Ast, J.P.L. Technical Report, #3 Contract No. 954852 (1979).
3. J.S. Hanoka, Solar Cells, 1, 123 (1979).
4. D.E. Ioannov, J. Appl. Phys. D: Appl. Phys., 13, 611 (1980).
5. L.C. Kimerling and J.R. Patel, Appl. Phys. Lett., 34, 73 (1979).
6. H. Strunk and D.G. Ast, Proc. 38th EMSA, 38 323, (1980).
7. H. Föll and D.G. Ast, J.P.L. Technical Report #1 Contract No. 954852 (1978).
8. C.V.H.H. Rao, M.C. Cretella, F.V. Wald and K.V. Ravi, J. Cryst. Growth 50, 311 (1980).
9. C.V. Hari Rao, H.E. Bates and K.V. Ravi, J. Appl. Phys., 47, 2614 (1976).
10. K. Yang, G.H. Schwuttke and T.F. Ciszek, J. Cryst. Growth 50, 301 (1980).
11. K.V. Ravi, J. Cryst. Growth, 39, 1 (1977).
12. G.H. Schwuttke, T.F. Ciszek and A. Kran, J.P.L. Technical Report #3, Contract No. 954144 (March 1976).
13. L.C. Garone, C.V. Hari Rao, A.D. Morrison, T. Surek and K.V. Ravi, Appl. Phys. Lett. 29, 511 (1976).
14. F.V. Wald, Private communication (1980).
15. F. Wald, Electrochemical Soc. Meeting, St. Louis, May 1980.
16. J.A. Kohn, Am. Mineral, 41, 778 (1956).
17. W. Bollmann, Crystal Defects and Crystalline Interfaces, Springer-Verlag (1970).
18. J.A. Kohn, Am. Mineral., 43, 263 (1958).
19. J. Hornstra, Physica, 25, 409 (1959).
20. R.W. Balluffi, Y. Komen and T. Schober, Surf. Sci., 31, 68 (1972).
21. P.B. Hirsch, A. Howie, R.B. Nicholson, D.W. Pashley and M.J. Whelan, Electron Microscopy of Thin Crystals, London: Butterworth (1965).
22. Proc. Int. Symp., Dislocations in Tetrahedrally Co-ordinated Semiconductors, J. Physique Colloq - C6, 40, (1979).
23. P.B. Hirsch, J. Microsc., 118, 3 (1980).
24. H. Alexander, J. Physique Colloq - C6, 40, 1 (1979).
25. A. Bourret and J. Dessequx, J. Physique Colloq-C6, 40, 7 (1979).
26. J.P. Hirth and J. Lothe, Theory of Dislocations, McGraw Hill, New York (1968) pp 359-362.
27. J. Hornstra, J. Phys. Chem. Sol., 5, 129 (1958).

FIGURE CAPTIONS

1. Optical micrographs of etched ribbon surface Ribbon #2.

2. Optical micrograph of ribbon surface showing variation in grain orientations. Open circles mark areas analyzed by Laue X-ray and also orientations with respect to standard 001 stereographic projection (Courtesy of F. Stafford).

3. EBIC micrograph of typical EFG structure. Ribbon #2.

4. Higher magnification EBIC micrograph of area at top right of Figure 3.

5. EBIC micrograph showing dotted contrast along linear boundaries. Ribbon #3.

6. TEM micrograph (125 kv) of microtwins in E.F.G. ribbon. Ribbon #1.

7. High resolution structural image of a microtwin five atomic layers thick. (125 kv).

8. EBIC micrograph showing contrast near a SiC particle. Ribbon #4.

9. a) Bright field HVEM image of a microtwin containing dislocations. b) Same area with twin out of contrast. c) EBIC micrograph from the same area. g = diffraction vector - Ribbon #4.

10. a) EBIC micrograph showing dotted contrast. b) Optical micrograph of the same area showing interaction of microtwins. Ribbon #2.

11. a) Bright field HVEM micrograph of twin boundaries shown in Figure 10.
    b) Same area with one set of twin boundaries out of contrast.

12. Schematic sketch of the arrangement of twin boundaries shown in Figure 11.

13. Projection along the common <110> direction of twins indicated in Figure 12 showing the arrangement of atoms at the (111) (115) twin join.

14. HVEM micrographs of the same area as Figure 11. These were used to determine the nature of the dislocations in the twin boundaries, examples of which are marked in c).

a

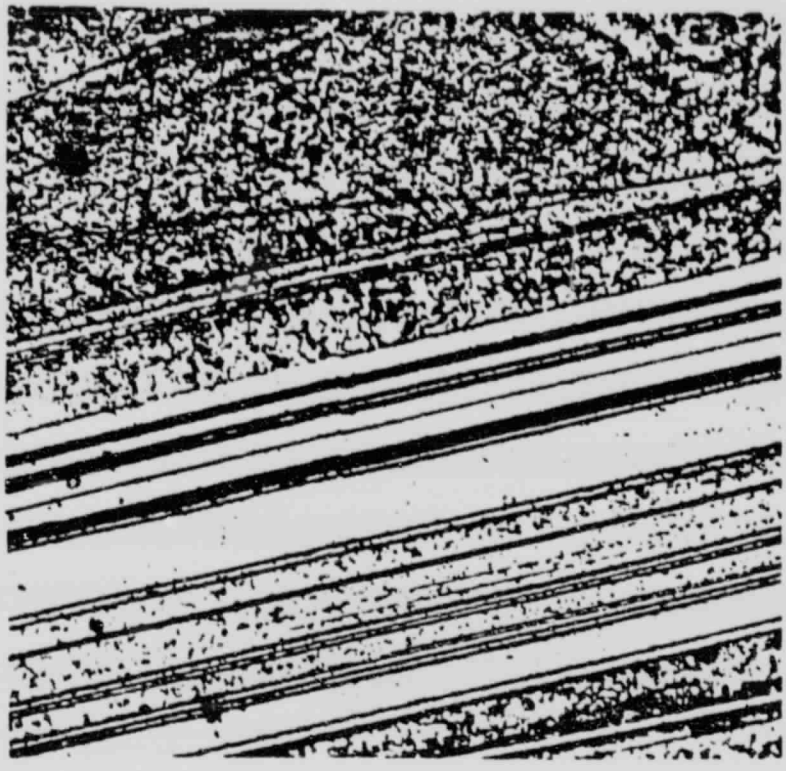

200μm

b

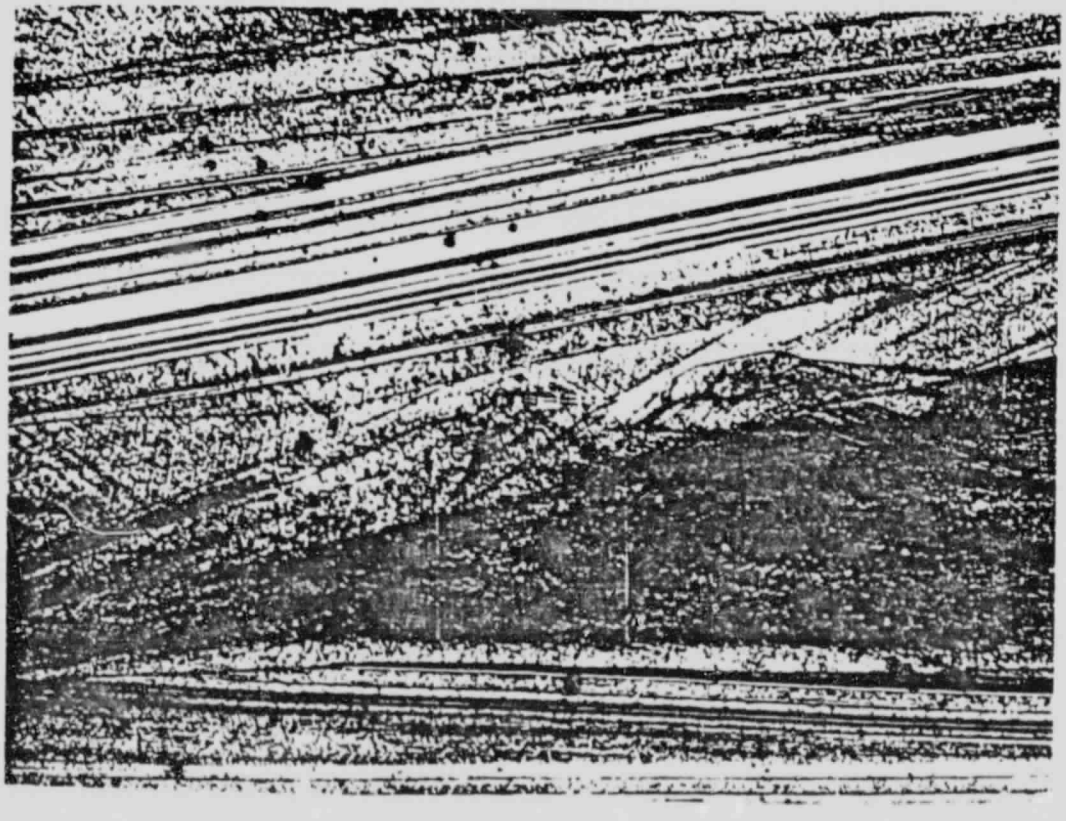

400μm

Figure. 1

Figure. 2

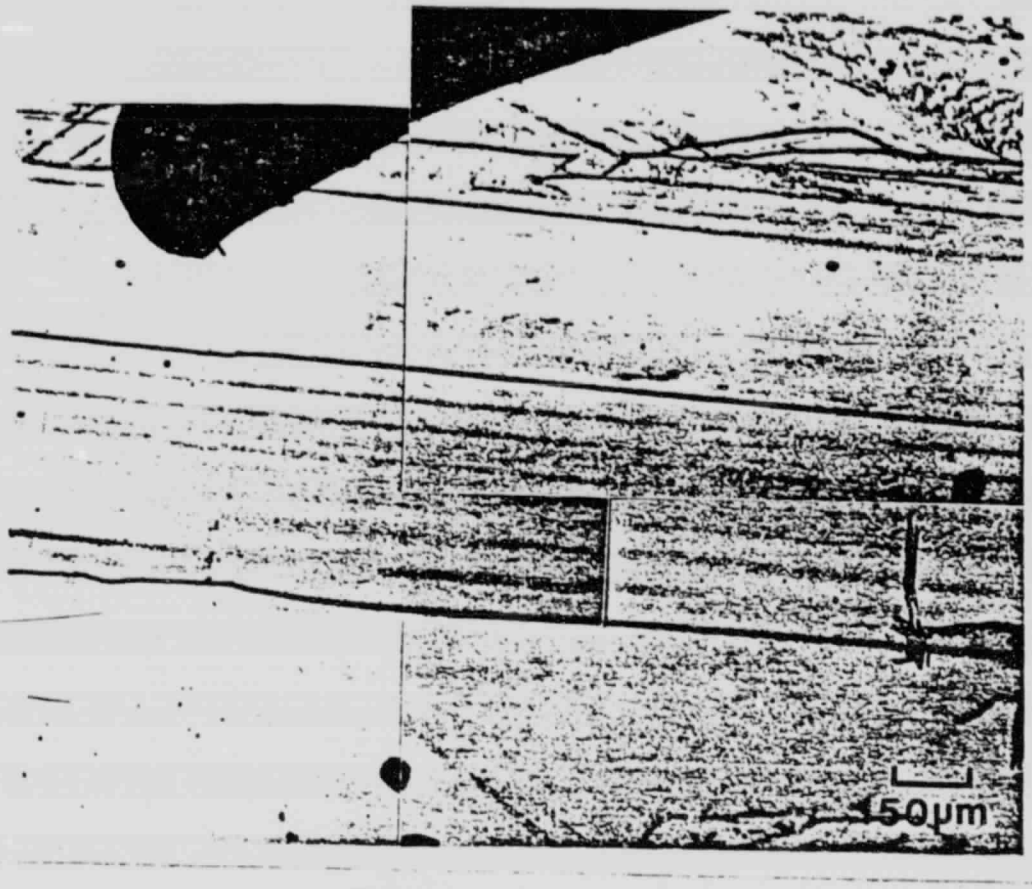

Figure. 3

Figure. 4

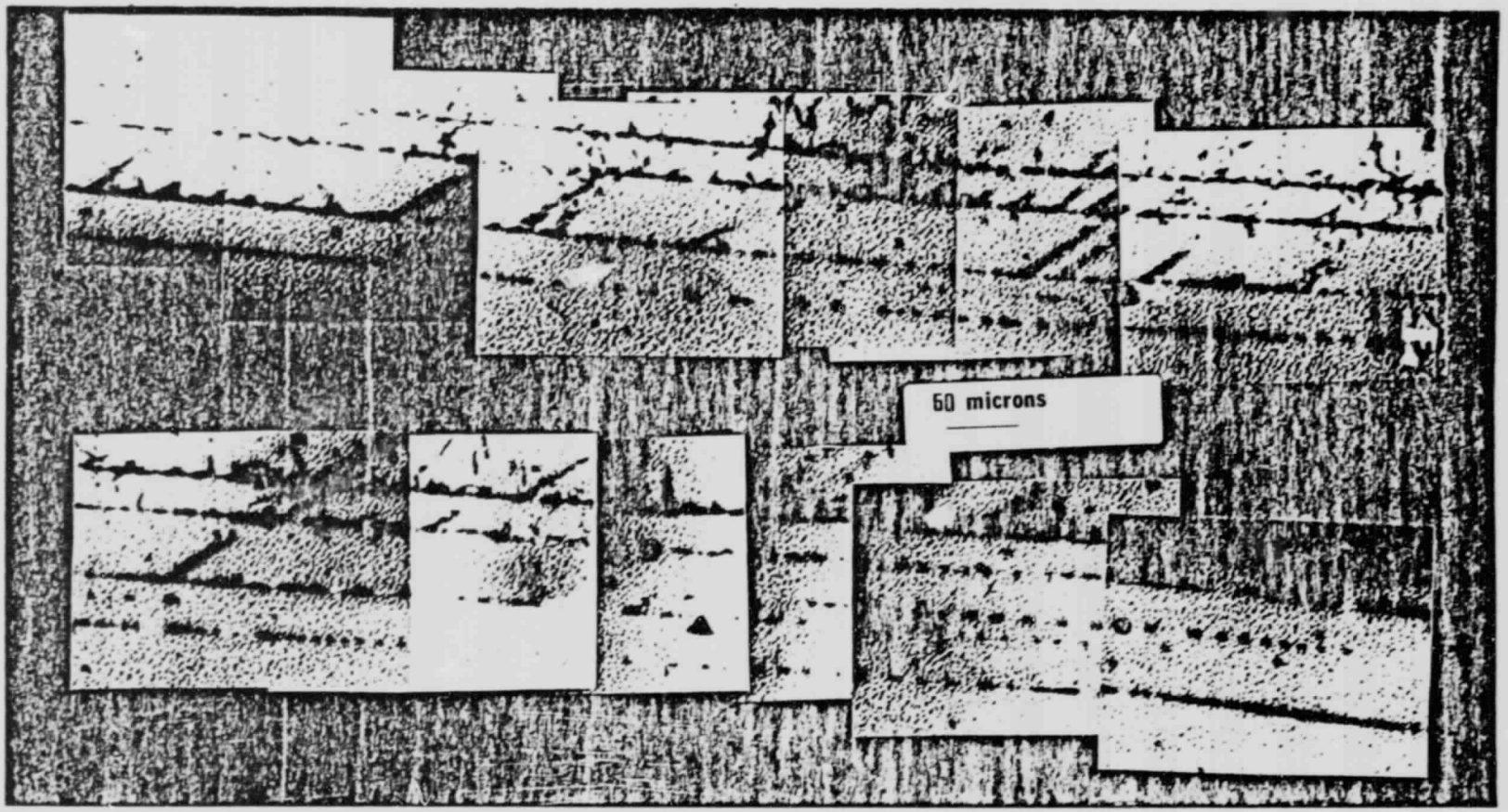

Figure. 5

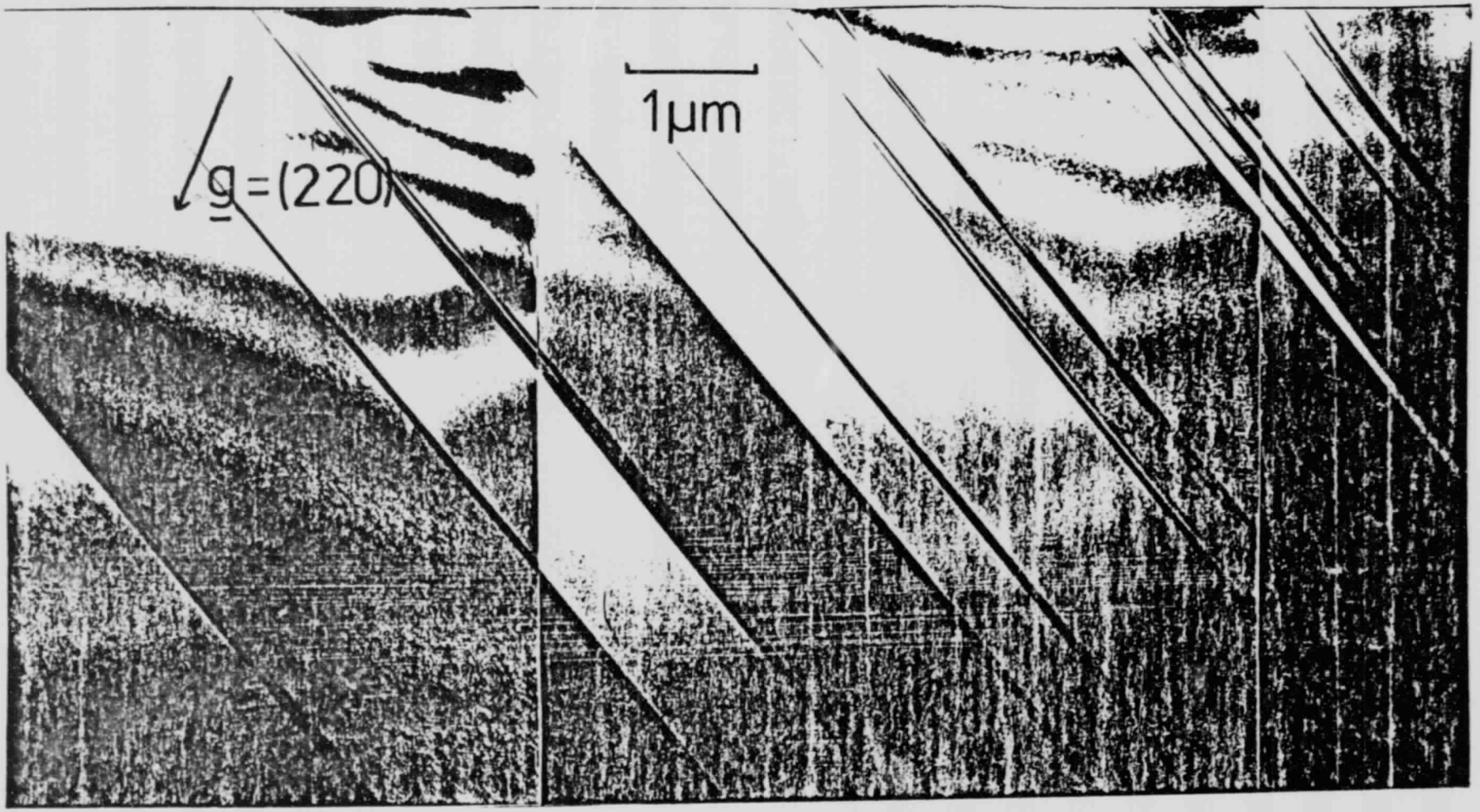

Figure. 6

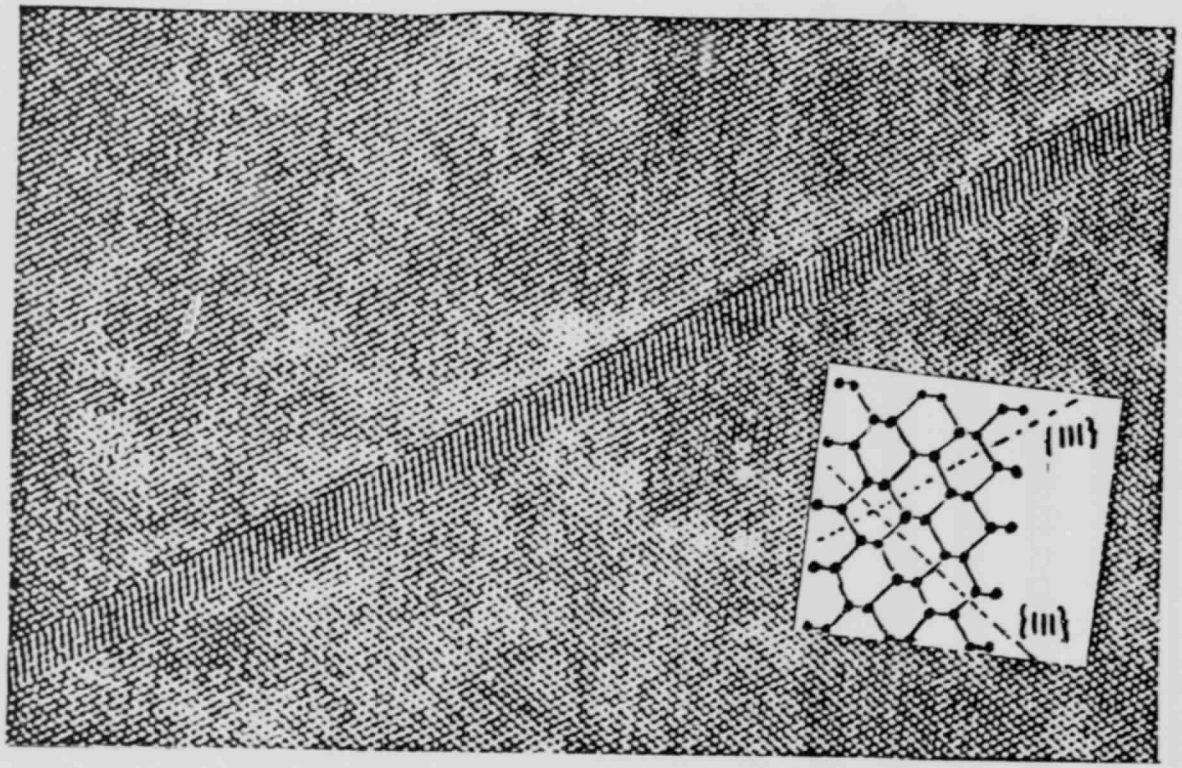

Figure. 7

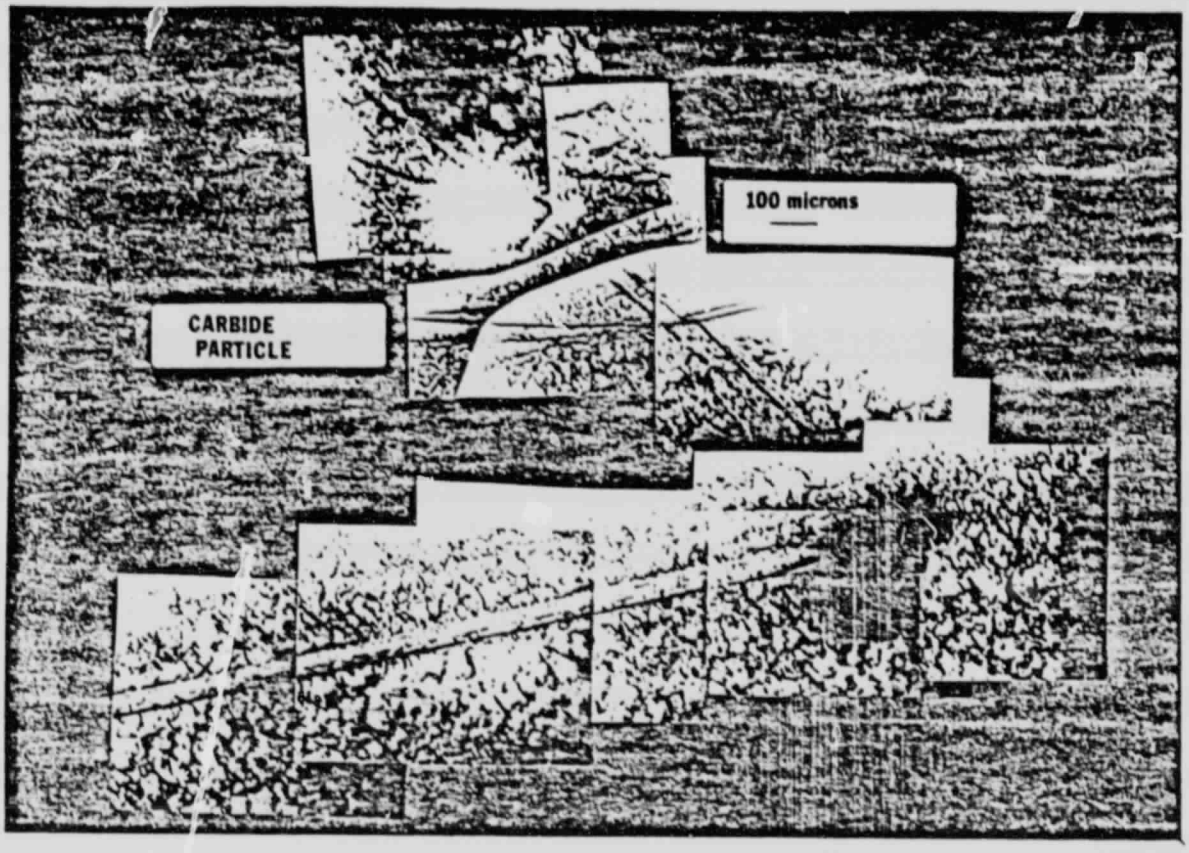

Figure. 8

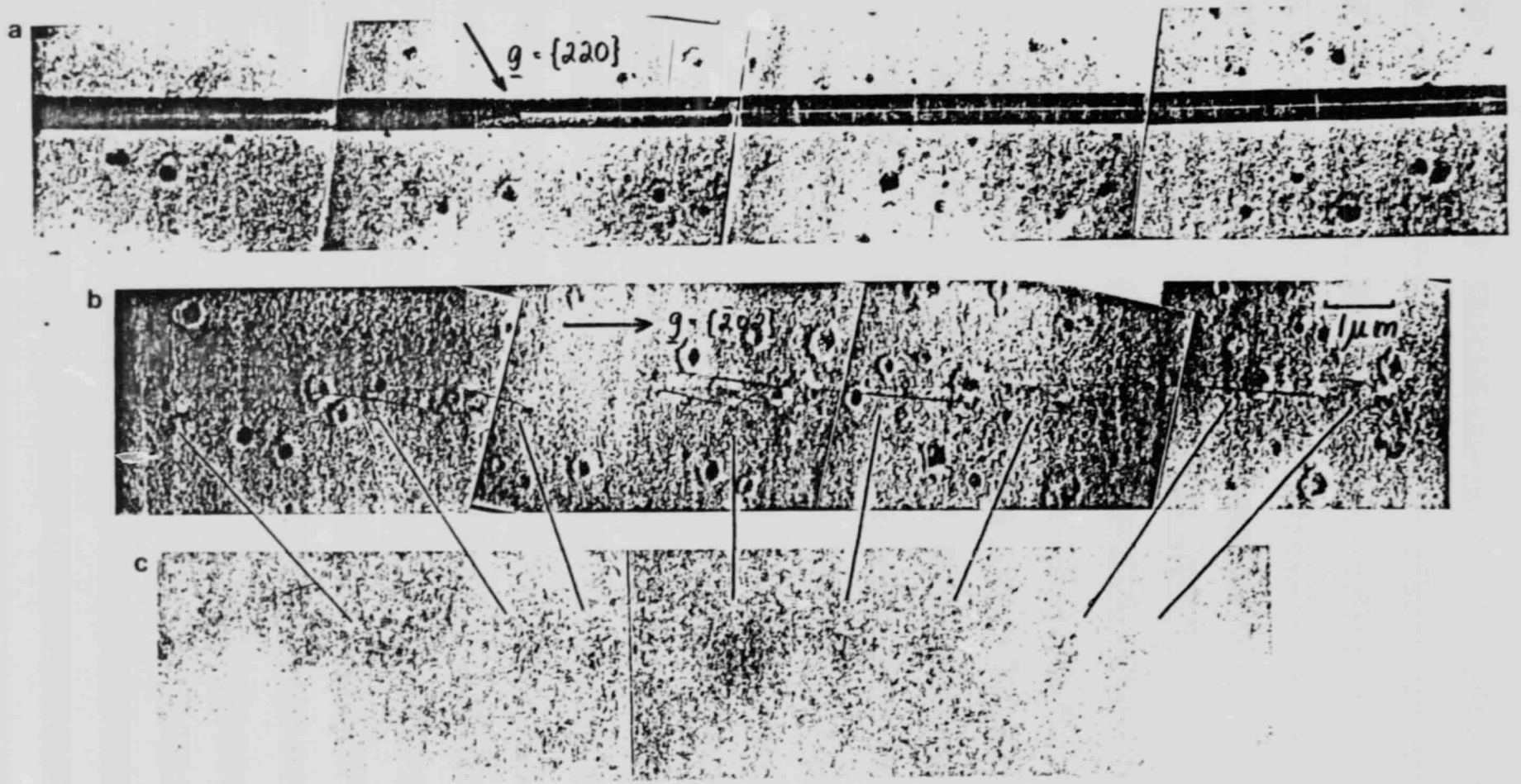

Figure. 9

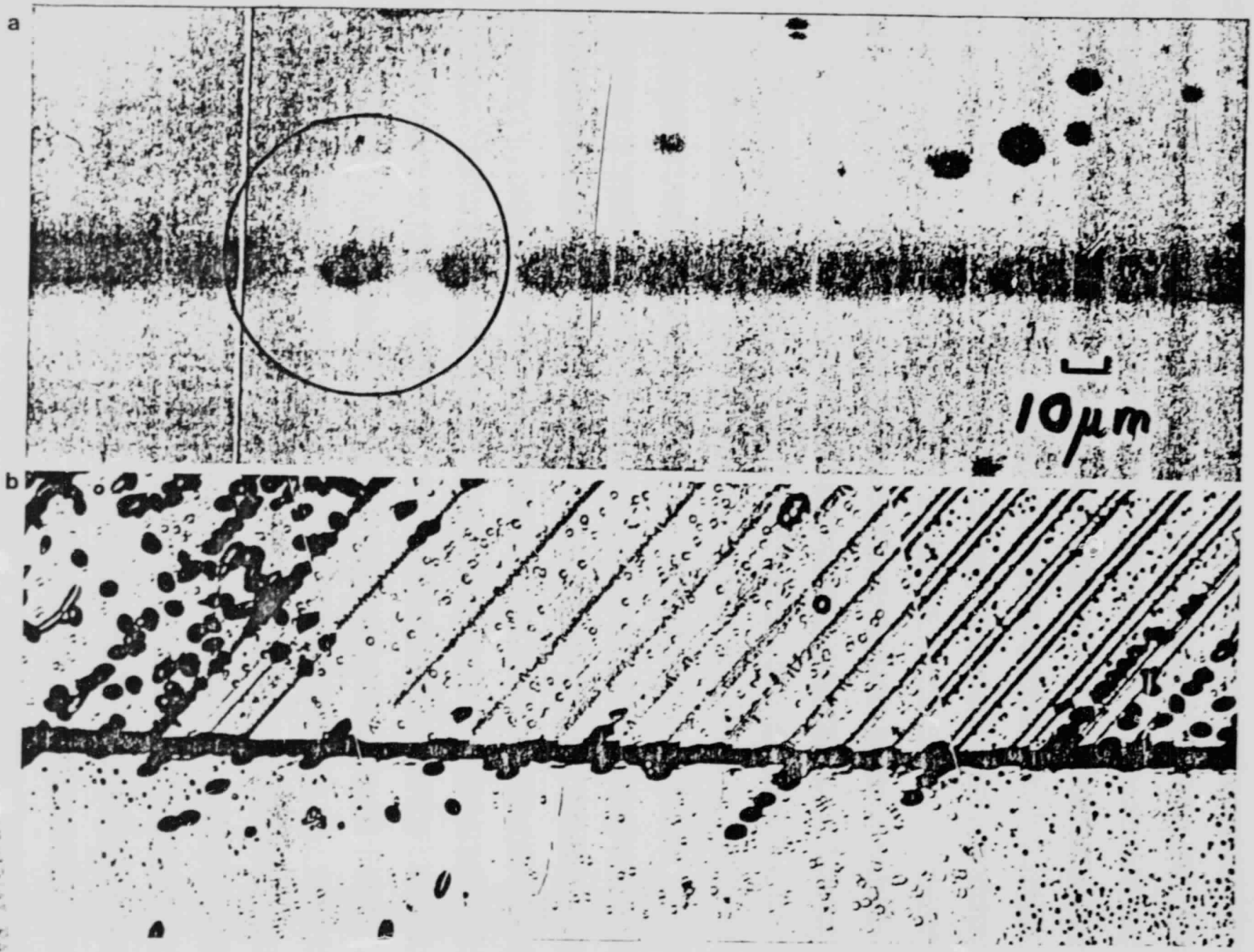

Figure. 10

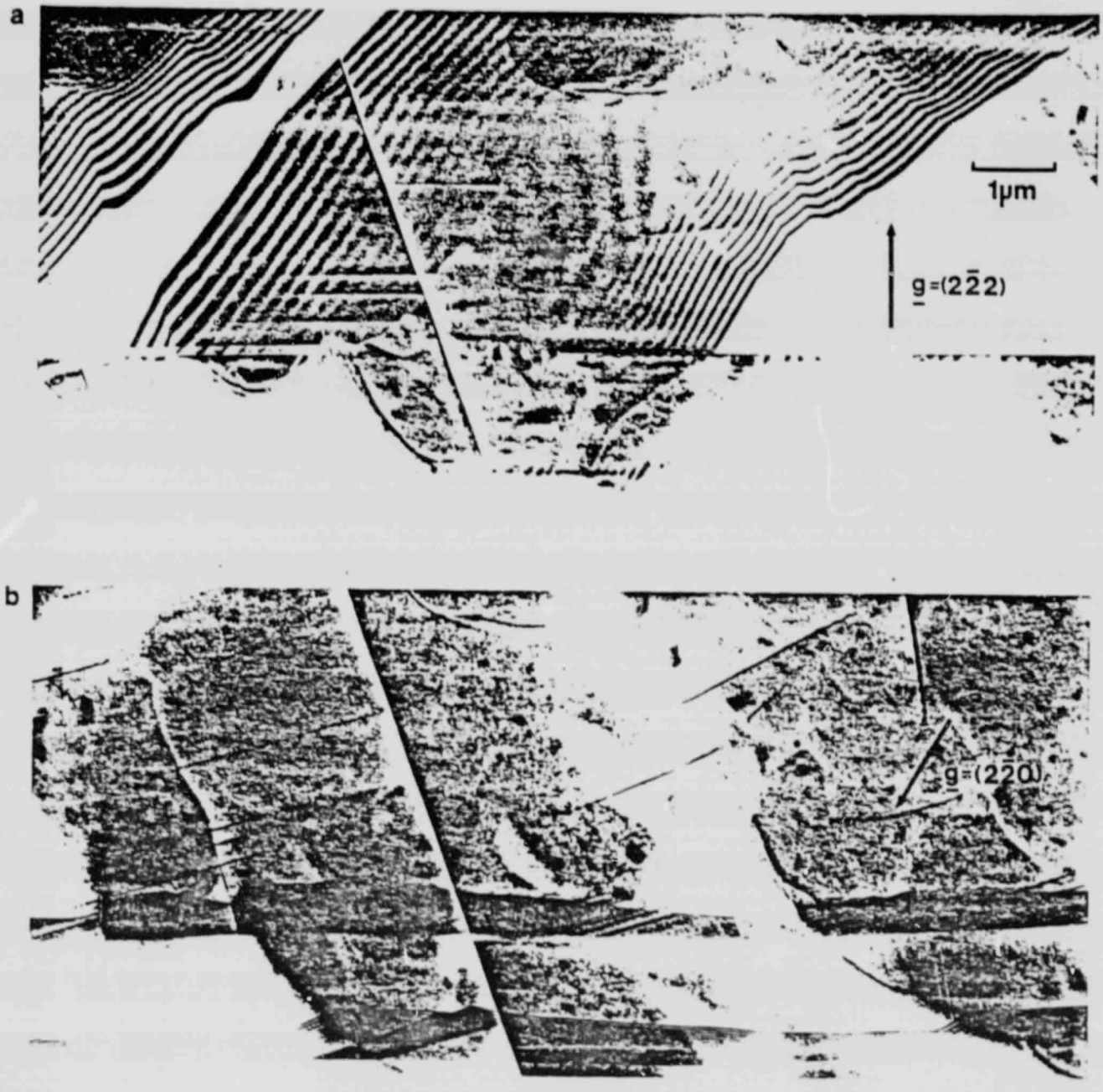

Figure.11

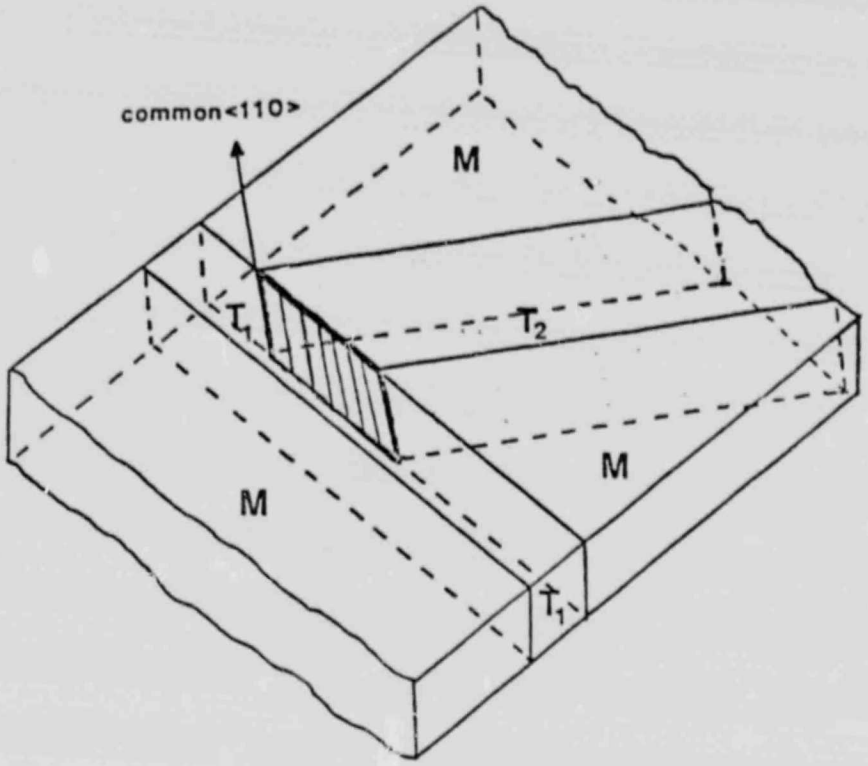

Figure. 12

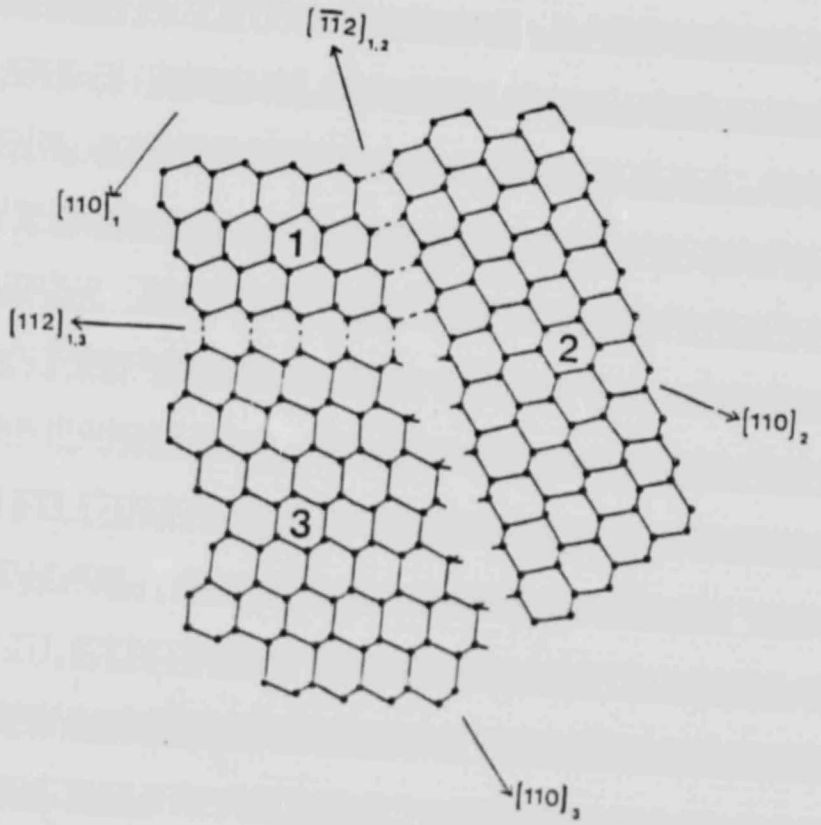

Figure. 13

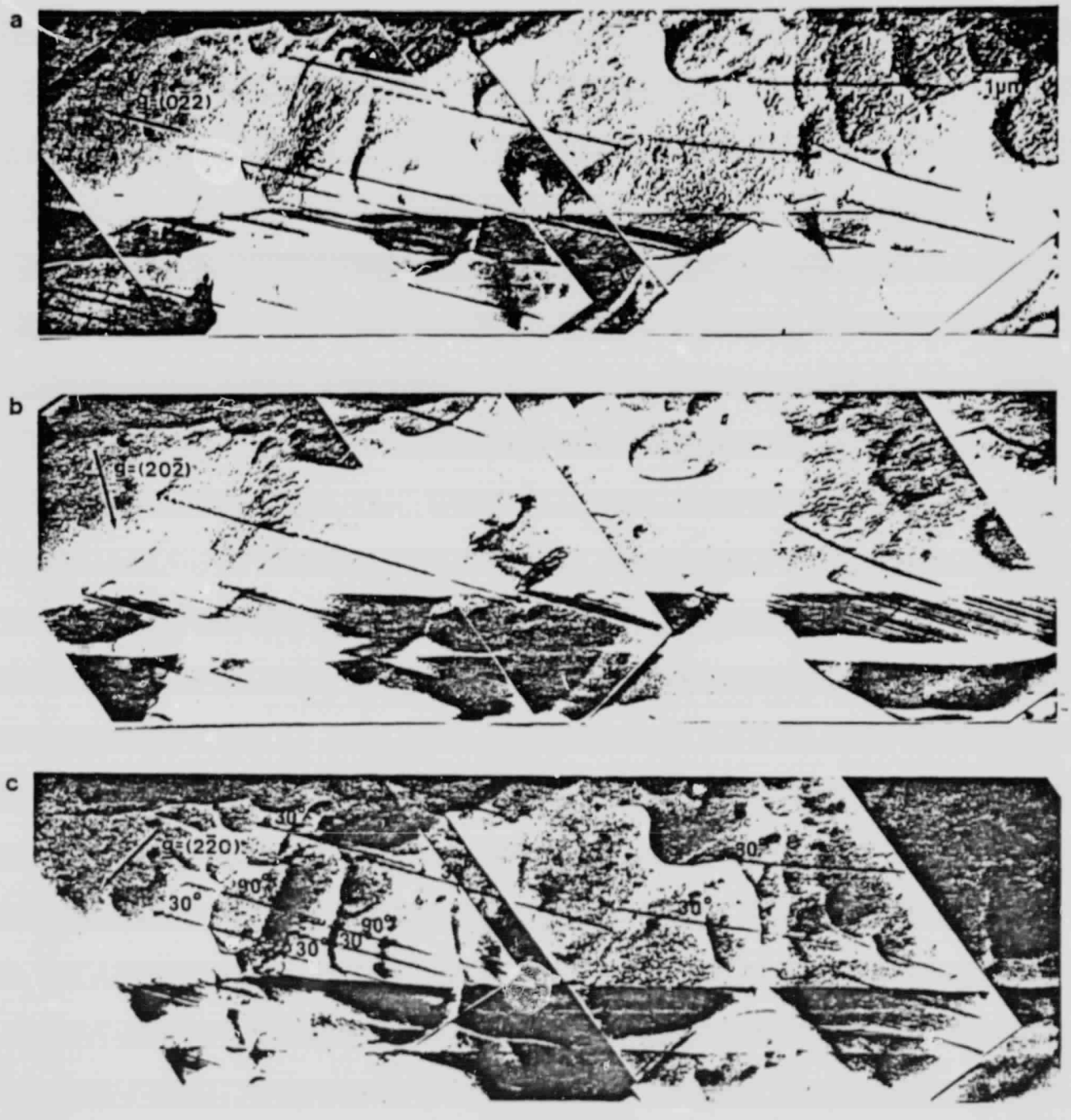

Figure.14